TECHNISCHE MECHANIK, 32, 1, (2012), 70 – 83
submitted: October 24, 2011

# Multi-Scale Simulation of Viscoelastic Fiber-Reinforced Composites

S. Staub, H. Andrä, M. Kabel, T. Zangmeister

*This paper presents an effective algorithm to simulate the anisotropic viscoelastic behavior of a fiber-reinforced composite including the influence of the local geometric properties, like fiber-orientation and volume fraction. The considered composites consist of a viscoelastic matrix which is reinforced by elastic fibers. The viscoelastic composite behavior results anisotropic due to the local anisotropic fiber-orientations. The influence of the local time-dependent viscoelastic properties are captured within two elastic microscopic calculations for each fiber-orientation in the composite part. These calculations can be performed within a preprocessing step, and thus no expensive, time-dependent viscoelastic multi-scale simulation has to be carried out to incorporate the local properties. The advantage of the presented approach is that the locally varying microscopic properties can be captured in a one-scale simulation within a commercial finite element tool like ABAQUS.*

## 1 Introduction

Since many years the relevance of fiber-reinforced composites is increasing considerably in numerous fields of engineering, such as automotive and aircraft industry, see Carbon Composites. Due to the high strength, and the possibility of lightweight construction these composites replace more and more traditional materials like steel. The mechanical properties of such fiber-reinforced polymers depend on the fiber volume fraction, the local fiber-orientation, the geometrical and elastic properties of the fibers as well as on the viscoelastic polymer matrix. In order to design these materials tailored to their specific applications it is important to understand and simulate the macroscopic effects depending on different microscopic settings in advance. Investigation of the relation between the microscopic properties like, e.g., fiber-orientation, and macroscopic effective properties, like e.g. stiffness, only in terms of laboratory experiments is much to time consuming and expensive. Therefore, in the work at hand a viscoelastic model to simulate the full macroscopic mechanical composite is presented, which is based on the geometrical, elastic and viscoelastic properties of the single constituents. Especially, the geometric properties, like the fiber volume fraction and the local fiber-orientation may vary remarkably in a macroscopic composite part due to the manufacturing process, which in many cases is injection or compression molding.

The work at hand is organized as follows: In Section 2 the governing equations of the considered microscopic boundary value problem are given and the applied microscopic isotropic viscoelastic model is reviewed. In a next step in Section 3 the basic steps of the applied homogenization are summarized and the considered composite which consists of a viscoelastic matrix reinforced by stiff elastic fibers, is describes in more detail and the viscoelastic behavior of the composite is studied numerically. Then, in Section 3.3 the isotropic viscoelastic model due to Kaliske and Rothert (1997) from the previous section is extended towards an anisotropic model, which captures the anisotropic relaxation behavior of the composite. The main advantage of the presented anisotropic model is the potential of incorporation of microscopic properties like fiber-orientation within a commercial finite element tool like ABAQUS. Finally, the presented concept is illustrated by numerical examples in Section 4.

Helpful references to literature are given in each section.

## 2 Linear Isotropic Viscoelastic Model

In order to give an algorithm for the numerical treatment of linear isotropic viscoelasticity the corresponding initial boundary value problem is reviewed. The equilibrium condition is given by

$$\operatorname{div} \boldsymbol{\sigma}(\boldsymbol{x},t) = \mathbf{0} \quad \forall (\boldsymbol{x},t) \in \Omega \times [0,T] \tag{1}$$

wherein $\boldsymbol{\sigma}(\boldsymbol{x},t)$ denotes the (time-dependent) stress tensor. The prescribed mixed boundary conditions on $\partial\Omega = \partial\Omega_d \cup \partial\Omega_t$ with $\partial\Omega_d \cap \partial\Omega_t = \emptyset$, can be summarized by

$$\left.\begin{array}{llcll} \textit{d}\text{isplacement} & \boldsymbol{u}(\boldsymbol{x},t) & = & \boldsymbol{u}^0(\boldsymbol{x}) & \text{in} \quad \partial\Omega_d \times [0,T] \\ \textit{t}\text{raction} & \boldsymbol{t}(\boldsymbol{x},t) & = & \boldsymbol{t}^0(\boldsymbol{x}) & \text{in} \quad \partial\Omega_t \times [0,T] \end{array}\right\}. \tag{2}$$

Thereby, $\boldsymbol{u}(\boldsymbol{x},t)$ denotes the displacement field, $\boldsymbol{n}$ the outward unit normal vector and $\boldsymbol{t}(\boldsymbol{x},t) := \boldsymbol{\sigma}(\boldsymbol{x},t) \cdot \boldsymbol{n}$ the traction vector. For further details on the initial boundary value problem the reader is referred to the standard textbooks in continuum mechanics, as Malvern (1969) or Holzapfel (2001).

The description of the mechanical problem is completed by the constitutive law which gives the relation between the stresses and the strains. In the work at hand a viscoelastic material behavior is considered and thus the stresses are connected to the strain rates in terms of the following convolution integral

$$\boldsymbol{\sigma}(\boldsymbol{x},t) = \int_0^t \mathbb{\Gamma}(\boldsymbol{x},t-s) : \frac{\partial \boldsymbol{\epsilon}(\boldsymbol{x},s)}{\partial s} \, \mathrm{d}s. \tag{3}$$

Therein, $\mathbb{\Gamma}(\boldsymbol{x},t-s)$ corresponds to the fourth-order relaxation tensor $\Gamma_{klmn}(\boldsymbol{x},t-s)$ of the viscoelastic material. The viscoelastic behavior is realized by a generalized Maxwell model consisting of a finite number $N$ Maxwell elements. Then, the normalized relaxation function is

$$\Psi(t) = 1 + \sum_{j=1}^{N} \gamma_j \exp\left(-\frac{t}{\tau_j}\right). \tag{4}$$

Thereby, $\gamma_j$, $j = 1, \dots N$ represent the normalized relaxation coefficients, i.e., in the one-dimensional case $\gamma_j = \dfrac{E_j}{E_\infty}$, whereby $E_j$ denotes the modulus of the Maxwell element $j$ and $E_\infty$ the longterm modulus, i.e., the elastic or Young's modulus. $\tau_j$ are the corresponding relaxation times.

First, an isotropic viscoelastic matrix material is considered. Although many polymers show different relaxation times under tensile- and compression-loading, here a constant Poisson's ratio is assumed, which together with the isotropy yields that all components have the same relaxation behavior and thus

$$\mathbb{\Gamma}(t) = \Psi(t)\, \mathbb{C}^r = \mathbb{C}^r + \sum_{j=1}^{N} \gamma_j \exp\left(-\frac{t}{\tau_j}\right) \mathbb{C}^r \tag{5}$$

is valid, whereby $\mathbb{C}^r$ corresponds to the relaxed stiffness tensor, i.e., in terms of the elastic stresses $\boldsymbol{\sigma}_0$ at $\lim t \to \infty$ holds $\mathbb{C}^r = \lim\limits_{t\to\infty} \dfrac{\partial \boldsymbol{\sigma}(t)}{\partial \boldsymbol{\epsilon}(t)}$.

Insertion of (5) into (3) yields the time-dependent total stress as

$$\boldsymbol{\sigma}(t) = \int_0^t \left[1 + \sum_{j=1}^{N} \gamma_j \exp\left(-\frac{t-s}{\tau_j}\right)\right] \mathbb{C}^r : \frac{\partial \boldsymbol{\epsilon}(s)}{\partial s} \, \mathrm{d}s \tag{6}$$

Thus, the total stress can be decomposed into an elastic and a viscoelastic part via

$$\boldsymbol{\sigma}(t) = \int_0^t \mathbb{C}^r : \frac{\partial \boldsymbol{\epsilon}(s)}{\partial s} \, \mathrm{d}s + \int_0^t \sum_{j=1}^{N} \gamma_j \exp\left(-\frac{t-s}{\tau_j}\right) \mathbb{C}^r : \frac{\partial \boldsymbol{\epsilon}(s)}{\partial s} \, \mathrm{d}s \tag{7}$$

By application of the definition of the elastic stress $\boldsymbol{\sigma}_0(t) = \mathbb{C}^r : \boldsymbol{\epsilon}(t)$ and permutation of the integration, the summation equation (7) can be rewritten as

$$\boldsymbol{\sigma}(t) = \boldsymbol{\sigma}_0(t) + \sum_{j=1}^{N} \underbrace{\int_0^t \gamma_j \exp\left(-\frac{t-s}{\tau_j}\right) : \frac{\partial \boldsymbol{\sigma}_0(s)}{\partial s}\, \mathrm{d}s}_{=:\boldsymbol{h}_j(t)}. \tag{8}$$

Thereby, the second term of the right hand side can be identified with stress-like internal variables $\boldsymbol{h}_j(t)$.

In a next step, a discretization in time is carried out and according to the work by Kaliske and Rothert (1997) a multiplicative split

$$\exp\left(-\frac{t^{n+1}}{\tau_j}\right) = \exp\left(-\frac{t^n + \Delta t^{n+1}}{\tau_j}\right) = \exp\left(-\frac{t^n}{\tau_j}\right) \exp\left(-\frac{\Delta t^{n+1}}{\tau_j}\right) \tag{9}$$

is performed in terms of the actual time step $\Delta t^{n+1}$ which yields a recursive update of the internal variables via

$$\boldsymbol{h}_j^{n+1} = \exp\left(-\frac{\Delta t^{n+1}}{\tau_j}\right) \boldsymbol{h}_j^n + \gamma_j \int_{t^n}^{t^{n+1}} \exp\left(-\frac{t^{n+1}-s}{\tau_j}\right) : \frac{\partial \boldsymbol{\sigma}_0(s)}{\partial s}\, \mathrm{d}s. \tag{10}$$

In order to solve the viscoelastic problem within a standard finite element scheme a discretized version of the constitutive law, which yields the total stresses as a function of the strains, and the corresponding viscoelastic stiffness tensor $\mathbb{C}^{vel}(t)$ are required. Due to the fact that the considered viscoelastic law is time-dependent, the stresses and the stiffness tensor are updated in each time step $\Delta t^n$.

The elastic stresses in each time step are obtained in terms of the elastic stiffness tensor via

$$\boldsymbol{\sigma}_0^{n+1} = \mathbb{C}^r : \boldsymbol{\epsilon}^{n+1}. \tag{11}$$

According to equation (8) the total stresses in each time step read

$$\boldsymbol{\sigma}^{n+1} = \boldsymbol{\sigma}_0^{n+1} + \sum_{j=1}^{N} \boldsymbol{h}_j^{n+1} \tag{12}$$

whereby the update of the discrete internal variables are obtained by a discretization and an analytical integration of (10) which yields

$$\boldsymbol{h}_j^{n+1} = \exp\left(-\frac{\Delta t^{n+1}}{\tau_j}\right) \boldsymbol{h}_j^n + \gamma_j \frac{1 - \exp\left(-\frac{\Delta t^{n+1}}{\tau_j}\right)}{\frac{\Delta t^{n+1}}{\tau_j}} \left[\boldsymbol{\sigma}_0^{n+1} - \boldsymbol{\sigma}_0^n\right]. \tag{13}$$

Finally, the viscoelastic stiffness matrix is achieved as the derivative of the total stresses with respect to the strains

$$\mathbb{C}^{vel,n+1} := \frac{\partial \boldsymbol{\sigma}^{n+1}}{\partial \boldsymbol{\epsilon}^{n+1}} = \left[1 + \sum_{j=1}^{N} \gamma_j \frac{1 - \exp\left(\frac{\Delta t^{n+1}}{\tau_j}\right)}{\frac{\Delta t^{n+1}}{\tau_j}}\right] \mathbb{C}^r. \tag{14}$$

Therein, the first term on the right-hand side can be identified with the discrete relaxation function, i.e.

$$\Psi^{n+1} = 1 + \sum_{j=1}^{N} \gamma_k \frac{1 - \exp\left(\frac{\Delta t^{n+1}}{\tau_j}\right)}{\frac{\Delta t^{n+1}}{\tau_j}}, \tag{15}$$

is valid. Therefore, equation (14) reduces to

$$\mathbb{C}^{vel,n+1} = \Psi^{n+1}\, \mathbb{C}^r. \tag{16}$$

Initialization

- elastic stress and internal variables

$$\boldsymbol{\sigma}_0^0 = \boldsymbol{\sigma}_0^r \quad \text{and} \quad \boldsymbol{h}_j^0 = \boldsymbol{h}_j^* \tag{I}$$

For each time step $\Delta t^n$

- calculate the elastic stress by using given total strain

$$\boldsymbol{\sigma}_0^{n+1} = \mathbb{C}^r : \boldsymbol{\epsilon}^{n+1} \tag{II}$$

- update the internal (stress-like) variables

$$\boldsymbol{h}_j^{n+1} = \exp\left(-\frac{\Delta t^{n+1}}{\tau_j}\right)\boldsymbol{h}_j^n + \gamma_j \frac{1-\exp\left(-\frac{\Delta t^{n+1}}{\tau_j}\right)}{\frac{\Delta t^{n+1}}{\tau_j}}\left[\boldsymbol{\sigma}_0^{n+1} - \boldsymbol{\sigma}_0^n\right] \tag{III}$$

- update the total stress

$$\boldsymbol{\sigma}^{n+1} = \boldsymbol{\sigma}_0^{n+1} + \sum_{j=1}^{N} \boldsymbol{h}_j^{n+1} \tag{IV}$$

- calculate the viscoelastic stiffness tensor

$$\mathbb{C}^{vel,n+1} = \Psi^{n+1}\,\mathbb{C}^r \quad \text{with} \quad \Psi^{n+1} = 1 + \sum_{j=1}^{N} \gamma_j \frac{1-\exp\left(\frac{\Delta t^n}{\tau_j}\right)}{\frac{\Delta t^n}{\tau_j}} \tag{V}$$

Figure 1: Time integration of viscoelastic material model

The necessary steps to calculate the total stresses and the viscoelastic stiffness matrix in each time step is summarized in Figure 1. These quantities can be applied as constitutive law in every standard finite element analysis software.

## 3 Linear Anisotropic Viscoelastic Model for Fiber-reinforced Composites

In the work at hand a macroscopic viscoelastic finite element simulation of a fiber-reinforced composite is carried out. Due to the fact that many parts in engineering applications are manufactured by injection molding, the fiber distribution is not homogeneous in each area. Therefore, the macroscopic simulation should take account of the local fiber-orientation and fraction in each element. In the current work a procedure is developed, which captures the influence of local fiber orientation within a preprocessing step. The macroscopic viscoelastic simulation, which here is performed by application of the commercial tool ABAQUS (www.simulia.com), then is able to capture this dependency without performing a full two-scale simulation, as given e.g. by the $FE^2$ scheme, see ,e.g., Feyel and Chaboche (2000), Kouznetsova et al. (2001), and Ricker (2011). Thus, the required simulation costs are reduced drastically, despite the fact that the influence of the micro structure is incorporated.

In the following a polypropylene (PP) polymer matrix reinforced by short circular glass fibers is considered. The glass fibers are assumed to behave linear elastic with a Young's modulus of $E = 73$ GPa and a Poisson's ratio $\nu = 0.23$. The matrix material is modeled by a linear viscoelastic constitutive law which is approximated by a chain of generalized Maxwell-elements. The number of Maxwell-elements $N$ has been set to 24, and the normalized relaxation coefficients $\gamma_k$ and the corresponding relaxation times $\tau_k$ have been fitted to master curves of storage and loss modulus, which have been determined in experiments. Within these experiment the short-term (unrelaxed) Young's modulus of the matrix resulted in $E^u = 2.75$ GPa and the long-term (relaxed) modulus in $E^r = 0.32$ GPa. The Poisson's ratio of the matrix is assumed constant in time (to fulfill (5)) at $\nu = 0.44$. For more on the need or expendability of time-dependent Poisson's ratios the reader is referred to Lakes and Wineman (2006).

First, the necessary background on homogenization theory is reviewed shortly.

### 3.1 Homogenization and Effective Properties

In order to determine the effective relaxation of the composite an averaging procedure is carried out. Therefore, the effective macro stresses and strains are defined as

$$\boldsymbol{\Sigma}(t) :=< \boldsymbol{\sigma}(\boldsymbol{x},t) > \quad \text{and} \quad \boldsymbol{E}(t) =< \boldsymbol{\epsilon}(\boldsymbol{x},t) > . \tag{17}$$

Therein, the averaging operator is given by the following volume averaging

$$< \bullet >:= \frac{1}{V}\int_V \bullet \, \mathrm{d}V. \tag{18}$$

The boundary conditions which give the scale-transition between the macro- and the micro-scale are chosen such that the energy equivalence principle

$$\boldsymbol{\Sigma} : \boldsymbol{E} =< \boldsymbol{\sigma} : \boldsymbol{\epsilon} >, \tag{19}$$

proposed by Hill (1963), is valid. This can be achieved, e.g., by application of periodic, mixed or Dirichlet boundary conditions. For further details on the scale-transition the reader is referred to literature on homogenization techniques, e.g. Nemat-Nasser and Hori (1999) and Mura (1987). In case of a viscoelastic material the energy density $< \boldsymbol{\sigma} : \boldsymbol{\epsilon} >$ is a transient quantity, i.e., the effective stiffness tensor $\mathbb{C}$ is obtained in each time step via

$$\boldsymbol{\Sigma}(t) = \mathbb{C}(t) : \boldsymbol{E}. \tag{20}$$

The elastic coefficients of the fourth-order tensor $\mathbb{C}$ can be computed by application of six loadcases (three orthogonal tension- and three orthogonal shear-load cases) to the underlying micro-structure. Thus, in each timestep six boundary value problems have to be solved to obtain the macroscopic relaxation of a composite. In case of periodic or Dirichlet boundary conditions the resulting global stiffness tensor is the same for all six loadcases.

In order to reduce the number of computations, focus is out onto the relaxation behavior of a viscoelastic matrix reinforced by stiff elastic fibers. Therefore, in a next step the relaxation behavior of fiber-reinforced composites is studied numerically.

### 3.2 Numerical Study on Relaxation Behavior of Fiber-reinforced Composites

Initially, microscopic volume elements for given fiber fractions and orientations are generated by the software package GeoDict (see Wiegmann et al. (2006) and www.geodict.com). This software package allows the automatic generation a random fiber distributions based on parameters like fiber volume fraction, orientation, thickness and length. A microscopic geometry is depicted exemplary in Figure 2. In this example a fiber volume fraction of

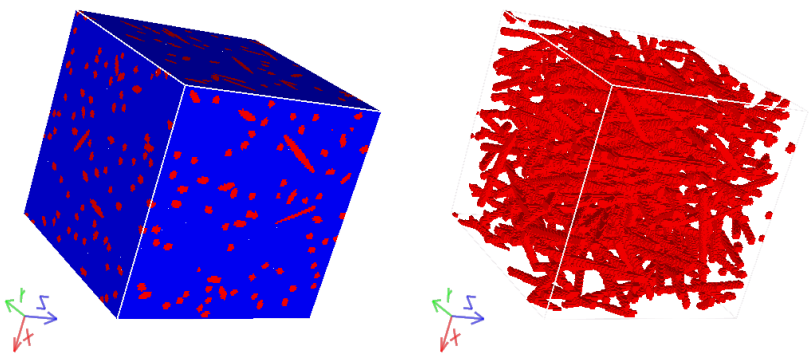

Figure 2: Microscopic volume element consisting of matrix reinforced by fibers, on the right-hand side only the fibers are displayed

10 % is considered. The placement of the fibers is performed periodically and it is assumed that the fibers do not percolate which is ensured by a minimum distance of two voxels between two neighboring fibers. All fibers have

the length $300\,\mu$m and the diameter $12\,\mu$m. Due to the periodicity of the structure the same fibers are cut at the boundary and continue at the opposite boundary. The contemplated volume element is discretized in $64^3$ voxels which for the applied voxel length of $6\,\mu$m results in a length of $384\,\mu$m in each direction.

The direction of the fibers is characterized by the fiber-orientation tensor according to Advani and Tucker (1987). The influence of the fiber-orientation onto the elastic properties is for example studied in Iorga et al. (2008). The (second-order) fiber-orientation tensor $\boldsymbol{Q}$ is obtained via the following averaging over the unit vectors $\boldsymbol{U}^n$ of each fiber $n$

$$\boldsymbol{Q} := \frac{1}{N} \sum_{n=1}^{N} \boldsymbol{U}^n \otimes \boldsymbol{U}^n \tag{21}$$

Additionally, the fourth-order fiber-orientation tensor

$$\mathbb{Q} := \frac{1}{N} \sum_{n=1}^{N} \boldsymbol{U}^n \otimes \boldsymbol{U}^n \otimes \boldsymbol{U}^n \otimes \boldsymbol{U}^n, \tag{22}$$

can be considered, but this topic goes beyond the scope of this work. The influence of the fourth-order tensor is e.g. regarded in Böhlke et al. (2010).

In the following example a fiber-reinforced viscoelastic matrix is considered. Thereby, four different realizations of the same micro-structure are generated by prescribing a target fiber-orientation and then their effective properties are averaged. The obtained averaged fiber-orientation tensor of the realizations reads

$$\boldsymbol{Q} = \begin{bmatrix} 0.741 & -0.007 & 0.030 \\ -0.007 & 0.015 & 0.000 \\ 0.030 & 0.000 & 0.244 \end{bmatrix}. \tag{23}$$

In Figure 3 the relaxation behavior of some components of the effective stiffness of the composite is plotted. Thereby, the unrelaxed and relaxed Young's moduli of the viscoelastic polymer matrix are given by $E^u = 2.75$ GPa and $E^r = 0.32$ GPa, whreas the elastic glass-fibers are characterized by $E = 73$ GPa. In all examples the viscoelatic relaxation is modeled by 24 Maxwell element, for which the parameters have been fitted to master-curves obtained by experiments.

Within Figure 3 the dashed lines correspond to the unrelaxed and relaxed modulus of the composite in the corresponding direction. Remarkably, all plotted relaxation curves have the same shape, but are arranged between different limits. The other components of the composite, which are left out here, show a similar relaxation behavior. Only, the $C_{11}$ component (Voigt notation), which corresponds to the main orientation of the fibers, shows an oscillating behavior at higher time scales. Due to the similarity in the shapes of the relaxation curves, according to the work of Krzikalla et al. (2011), the viscoelastic curves are normalized to values between 1 and 0, via

$$C_{ij}^{\text{norm}}(t) = \frac{C_{ij}(t) - C_{ij}^r}{C_{ij}^u - C_{ij}^r} \tag{24}$$

see Figure 4. Therein, the unmarked lines display the deviation between the normalized relaxation of the composite and the pure matrix material, which for the illustration is scaled by factor 5. The figure reveals that each component of the stiffness tensor behaves similarly to the normalized relaxation of the pure matrix material. In deBotton and Tevet-Deree (2004) it has been described already that for a viscoelastic matrix reinforced by stiff elastic fibers, the normalized relaxation curves are governed by the relaxation of the pure matrix material and that the matrix material relaxes slightly faster as the composite.

In order to complete these considerations, the influence of the stiffness contrast between the relaxed matrix and the fiber is considered. Figures 5 and 6 show the normalized relaxation of the stiffness tensor for different contrasts between the relaxed Young's modulus of the matrix and the fibers. The micro-structure is taken from the previous simulations, and again an arithmetic averaging over 4 realizations is performed. The Young's modulus of the fibers are $E_1 = 8$ GPa and $E_3 = 32$ GPa and for the matrix it holds $E^r = 0.32$ GPa. These figures reveal that the bigger the contrast between the stiffness of the matrix and the fiber the closer the normalized relaxation curves to the one

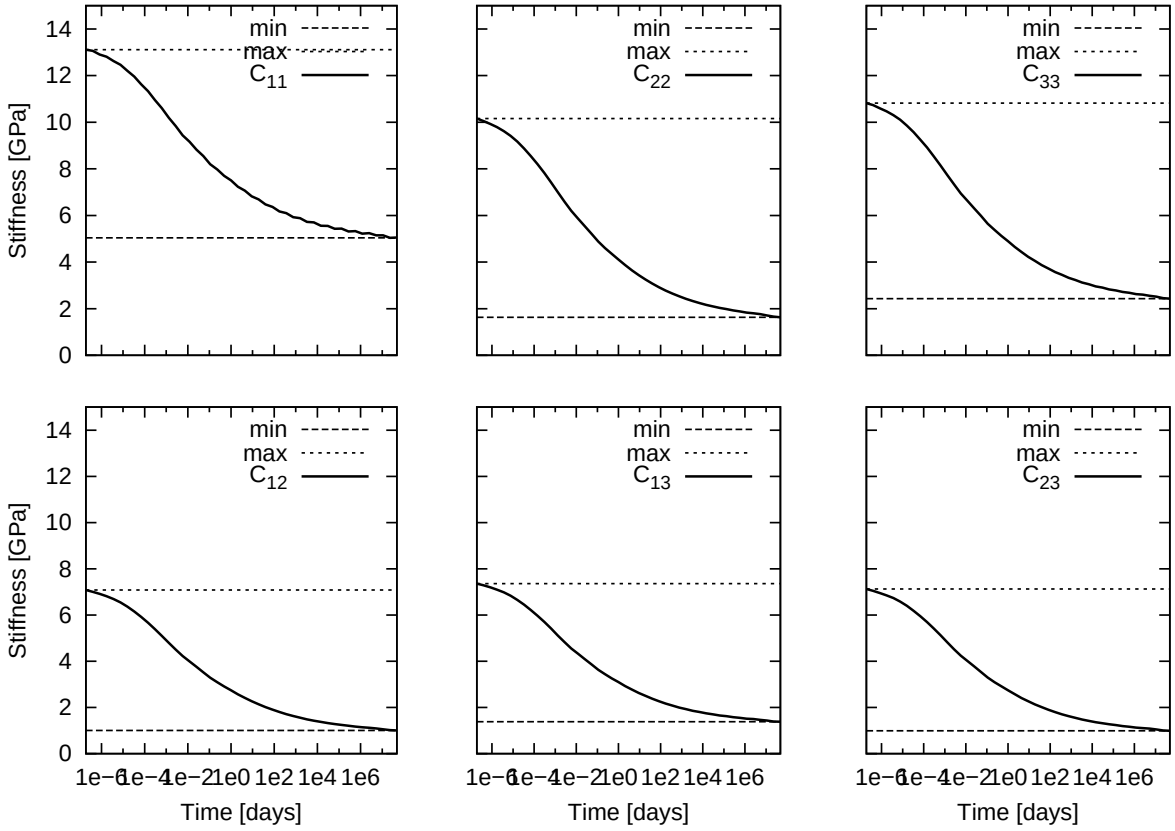


Figure 3: Relaxation of fiber-reinforced viscoelastic matrix with $E^u = 2.75$ GPa, $E^r = 0.32$ GPa, and elastic fiber modulus $E = 73$ GPa

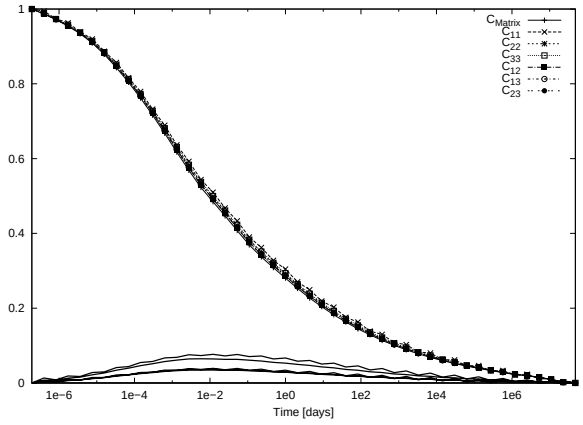


Figure 4: Normalized relaxation curves for fiber-reinforced viscoelastic matrix with $E^u = 2.75$ GPa, $E^r = 0.32$ GPa, and elastic fiber modulus $E = 73$ GPa

of the pure matrix material. Concludingly, for the regarded glass fibers with $E = 73$ GPa, the relaxation behavior of the composite can be assumed to be governed by the relaxation of the pure matrix material.

In the following, the algorithm from Section 2 is extended such that the anisotropic relaxation behavior of composites can be regarded.

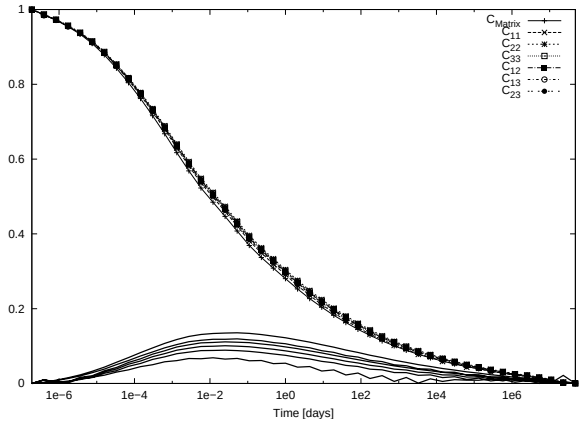


Figure 5: Normalized stiffnesses of matrix and composite with $E_1/E^r = 25$

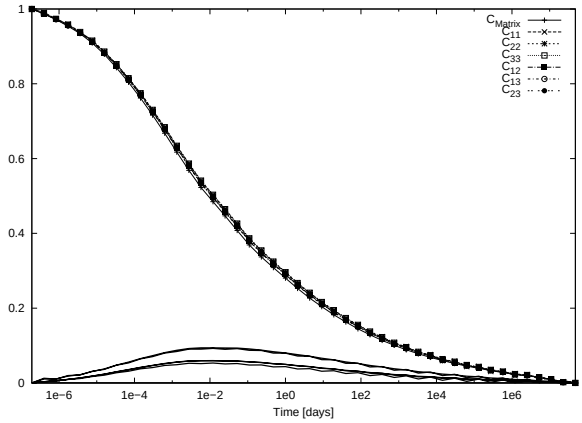


Figure 6: Normalized stiffnesses of matrix and composite with $E_3/E^r = 100$

### 3.3 Numerical Treatment of Anisotropic Relaxation of Fiber-reinforced Composites

In order to capture the anisotropic viscoelastic behavior of fiber-reinforced composites the relaxation tensor as given in equation 5 is defined component-wise as

$$\Gamma_{klmn}(t) = \Psi_{klmn}(t)\, C^r_{(klmn)} \tag{25}$$

where in each component of $\Psi_{klmn}$ is obtained via

$$\Psi_{klmn} = 1 + \sum_{j=1}^{N} \xi^j_{klmn} \exp\left(-\frac{t}{\tau_j}\right). \tag{26}$$

The relaxation coefficients $\xi^j_{klmn}$ need to guarantee the condition that the normalized relaxation behavior of the composite in each direction equals the normalized isotropic relaxation behavior of the pure matrix material according to the previous section. To this end focus is put onto the normalized relaxation $R^m$ which for the matrix and the composite is

$$R^m(t) := \frac{\Psi(t) - 1}{\sum\limits_{j=1}^{N} \gamma^j} = \frac{\Psi_{klmn}(t) - 1}{\sum\limits_{j=1}^{N} \xi^j_{(klmn)}} \quad \forall\, k, l, m, n, = 1, 2, 3. \tag{27}$$

Thus, at $t = 0$ it holds

$$R^m(0) = \frac{\Psi(0) - 1}{\sum_{j=1}^{N} \gamma^j} = \frac{\Psi_{klmn}(0) - 1}{\sum_{j=1}^{N} \xi^j_{(klmn)}} = 1 \quad \forall\, k, l, m, n, = 1, 2, 3, \tag{28}$$

which yields

$$\sum_{j=1}^{N} \xi^j_{klmn} = \sum_{j=1}^{N} \frac{\Psi_{klmn}(0) - 1}{\Psi(0) - 1} \gamma^j. \tag{29}$$

Insertion of $\Gamma_{klmn}(0) = C^u_{klmn}$ and equation (25) yield the following component-wise definition of the relaxation coefficients

$$\xi^j_{klmn} = \left[ \frac{C^u_{klmn}}{C^u_{(klmn)}} - 1 \right] \frac{\gamma_j}{\bar{\gamma}} \quad \text{with} \quad \bar{\gamma} = \sum_{i=1}^{N} \gamma_i. \tag{30}$$

Therefore, to include the influence of the local fiber orientation in each of the macroscopic element and to describe the corresponding anisotropic relaxation behavior two elastic simulations to determine $\mathbb{C}^u$ and $\mathbb{C}^r$ in each element are required.

The advantage of this procedure is that these elastic calculation can be performed in a preprocessing step. The effective unrelaxed and relaxed stiffness tensors then can be stored within a data base. Furthermore, to reduce the number of required simulations, interpolations of the stiffness tensors with respect to already simulated microscopic fiber orientations are possible. The required steps for the preprocessing are summarized in Figure 7.

In a next step the viscoelastic constitutive law from Section 2 is extended to anisotropic viscoelasticity based on the anisotropic relaxation coefficients $\xi^j_{klmn}$. Similar to the isotropic viscoelasticity, here only the determination of the total stresses in terms of the strains and the corresponding viscoelastic stiffness matrix is considered. This information is then used in a standard finite element code, as e.g. ABAQUS, to solve the macroscopic problem.

The anisotropic viscoelastic stresses result according to (3) and (5) then in

$$\Sigma_{kl}(t) = \int_0^t \left[ 1 + \sum_{j=1}^{N} \xi^j_{klmn} \exp\left( -\frac{t}{\tau_j} \right) \right] C^r_{klmn} : \frac{\partial \epsilon_{mn}(s)}{\partial s} \, \mathrm{d}s. \tag{31}$$

In order to simplify the notation, the anisotropic composite matrix for each Maxwell element is defined as

$$D^j_{klmn} := \xi^j_{klmn} C^r_{(klmn)}, \tag{32}$$

and thus (31) results in

$$\boldsymbol{\Sigma}(t) = \int_0^t \mathbb{C}^r + \sum_{j=1}^{N} \exp\left( -\frac{t}{\tau_j} \right) \mathbb{D}^j : \frac{\partial \boldsymbol{\epsilon}(s)}{\partial s} \, \mathrm{d}s. \tag{33}$$

Analogously to the isotropic viscoelasticity a split into the elastic and the viscoelastic part of the stresses yields

$$\boldsymbol{\Sigma}(t) = \boldsymbol{\Sigma}_0(t) + \sum_{i=1}^{N} \boldsymbol{H}_j(t), \tag{34}$$

where the anisotropic internal variables are

$$\boldsymbol{H}_j = \int_0^t \exp\left( -\frac{t}{\tau_j} \right) \mathbb{D}_j : \frac{\partial \boldsymbol{E}(s)}{\partial s} \, \mathrm{d}s. \tag{35}$$

Application of a multiplicative split (see equation (9)), discretization and analytical integration result in a recursive formula for the anisotropic internal variables

$$\boldsymbol{H}_j^{n+1} = \exp\left(-\frac{\Delta t^{n+1}}{\tau_j}\right) \boldsymbol{H}_j^n + \frac{1-\exp\left(-\frac{\Delta t^{n+1}}{\tau_j}\right)}{\frac{\Delta t^{n+1}}{\tau_j}} \mathbb{D}_j : \left[\boldsymbol{E}^{n+1} - \boldsymbol{E}^n\right] \tag{36}$$

Again, for the applied finite element scheme the viscoelastic tangent matrix is required which according to (10) is

$$\mathbb{C}_{aniso}^{vel,n+1} := \frac{\partial \boldsymbol{\Sigma}^{n+1}}{\partial \boldsymbol{E}^{n+1}} = \mathbb{C}^r + \sum_{j=1}^{N} \frac{1-\exp\left(-\frac{\Delta t^{n+1}}{\tau_j}\right)}{\frac{\Delta t^{n+1}}{\tau_j}} \mathbb{D}_j. \tag{37}$$

Therein, the relaxation function of each Maxwell element can be identified by

$$\Psi_j^{n+1} = \frac{1-\exp\left(-\frac{\Delta t^{n+1}}{\tau_j}\right)}{\frac{\Delta t^{n+1}}{\tau_j}}, \tag{38}$$

and thus (37) reduces to

$$\mathbb{C}_{aniso}^{vel,n+1} = \mathbb{C}^r + \sum_{j=1}^{N} \Psi_j^{n+1} \boldsymbol{D}_j. \tag{39}$$

The anisotropic viscoelastic material law for composites in summarized in Figure 8.

For each fiber orientation in the elements of the composite

- calculate the effective unrelaxed and relaxed stiffness tensors $\mathbb{C}^u$ and $\mathbb{C}^r$ by two elastic simulations
- for each Maxwell-Element $k$ of the matrix material
  - calculate the relaxation coefficients of the composite (by component):
    $$\xi_{klmn}^j = \left[\frac{C_{klmn}^u}{C_{(klmn)}^r} - 1\right] \frac{\gamma_j}{\widetilde{\gamma}} \quad \text{with} \quad \widetilde{\gamma} = \sum_{i=1}^{N} \gamma_i \tag{VI}$$
  - calculate the anisotropic composite matrix (by component):
    $$D_{klmn}^j = \xi_{klmn}^j \, C_{(klmn)}^r \tag{VII}$$

Figure 7: Preprocessing for anisotropic viscoelastic composite model

## 4 Numerical Examples

In the following section the viscoelastic behavior of a fiber-reinforced structure is simulated by two different approaches and the results are compared numerically. A standard viscoelastic approach as implemented in each finite element analysis tool is applied and compared to the model from the previous section which is able to capture the full anisotropic relaxation behavior with respect to the local fiber-orientation. Subsequently, the first approach is denoted as isotropic viscoelasticity, due to the fact that only the isotropic viscoelastic behavior of the matrix material governs the viscoelastic behavior of the composite. The second approach where in each direction of the composite the relaxation coefficients are scaled separately, is referred to as anisotropic viscoelasticity.

In the presented relaxation test a quarter of a stripe with hole as given in Figure 9 is considered. The microscopic fiber-orientation within this example is chosen in an academic way, i.e. unidirectional in-plane fibers are considered. The orientation of the fibers is changed stepwise within ten stripes across the stripe, from fibers which are parallel to the x-axis to fibers-parallel to the y-axis. In z-direction the fiber-orientation is kept constant. Also the fiber volume fraction is considered constant at 5%. As mentioned before a viscoelastic PP matrix is considered with short- and long-term moduli $E^u = 2.75$ MPa and $E^r = 0.32$ MPa. The Poisson's ratio is kept constant at $\nu = 0.44$. The linear elastic glass fibers are characterized by $E = 73$ GPa and $\nu = 0.32$. For the numerical relaxation experiment a displacement $u_y = 0.1$ mm is applied in longitudinal direction. This displacement is held

Initialization

- elastic stress and internal variables

$$\boldsymbol{\Sigma}_0^0 = \boldsymbol{\Sigma}_0^r \quad \text{and} \quad \boldsymbol{H}_j^0 = \boldsymbol{H}_j^* \tag{VIII}$$

For each time step $\Delta t^n$

- calculate the elastic stress by using the given total strain

$$\boldsymbol{\Sigma}_0^{n+1} = \mathbb{C}^r : \boldsymbol{E}^{n+1} \tag{IX}$$

- update the internal (stress-like) variables depending on the anisotropic relaxation

$$\boldsymbol{H}_j^{n+1} = \exp\left(-\frac{\Delta t^{n+1}}{\tau_j}\right) \boldsymbol{H}_j^n + \frac{1 - \exp\left(-\frac{\Delta t^{n+1}}{\tau_j}\right)}{\frac{\Delta t^{n+1}}{\tau_j}} \mathbb{D}_j : \left[\boldsymbol{E}^{n+1} - \boldsymbol{E}^n\right] \tag{X}$$

- update the total stress

$$\boldsymbol{\Sigma}^{n+1} = \boldsymbol{\Sigma}_0^{n+1} + \sum_{j=1}^{N} \boldsymbol{H}_j^{n+1} \tag{XI}$$

- calculate the viscoelastic stiffness tensor

$$\mathbb{C}_{aniso}^{vel,n+1} = \mathbb{C}^r + \sum_{j=1}^{N} \Psi_j^{n+1} \mathbb{D}_j \quad \text{with} \quad \Psi_j^{n+1} = \frac{1 - \exp\left(-\frac{\Delta t^{n+1}}{\tau_j}\right)}{\frac{\Delta t^{n+1}}{\tau_j}} \tag{XII}$$

Figure 8: Applied anisotropic viscoelastic composite model

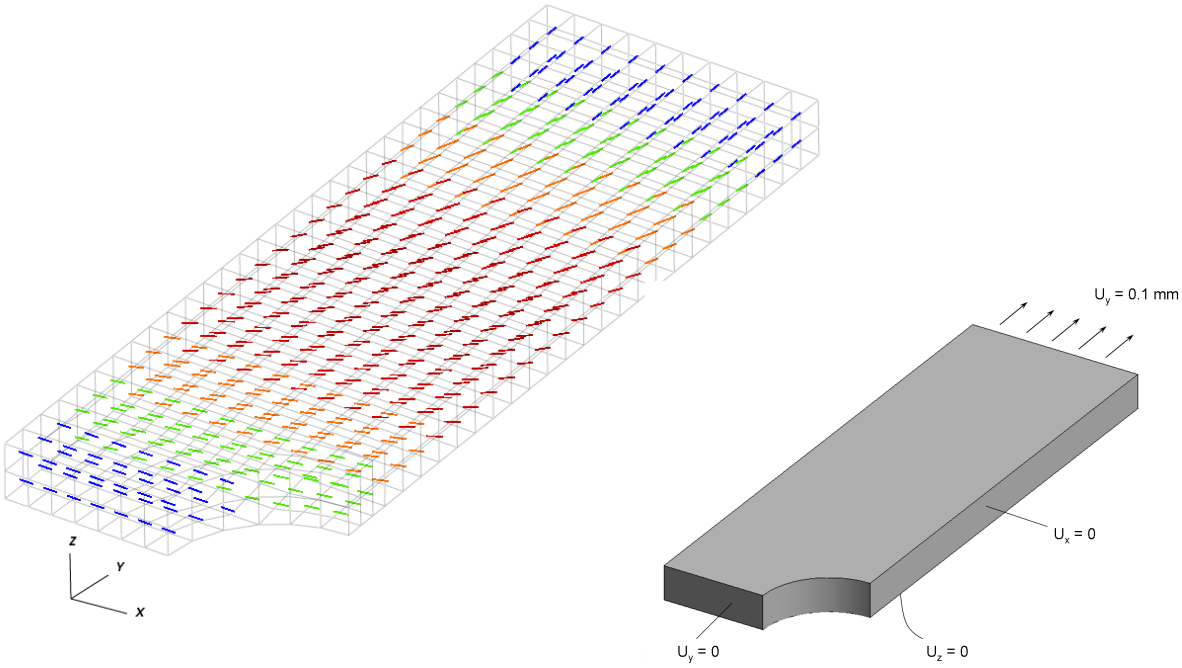


Figure 9: Illustration of the inhomogeneous fiber orientation and applied boundary conditions

for ten seconds and then released. Symmetry boundary conditions are applied to the structure. It is assumed that for each fiber-orientation in the macroscopic composite two elastic homogenization simulation have been carried out to determine the effective unrelaxed and relaxed tangent matrices $\mathbb{C}^u$ and $\mathbb{C}^r$. Furthermore, it has been incorporated that the normalized relaxation behavior of the composite is governed by the normalized matrix relaxation, according to Section 3.1.

For the isotropic viscoelastic model the relaxation coefficients $\gamma_j$ of the matrix material have been multiplied by

$$\left[\frac{C^u_{22}}{C^r_{22}} - 1\right] \frac{1}{\tilde{\gamma}} \quad \text{with} \quad \tilde{\gamma} = \sum_{i=1}^{N} \gamma_i \tag{40}$$

in order to scale the behavior of the composite at least in the direction of loading, such that the normalized relaxation behavior of matrix and composites coincide. Here, the effective matrices $C^r$ and $C^u$ of the mean fiber-orientation, i.e. fibers in a $45°$ angle to the x-axis, are used.

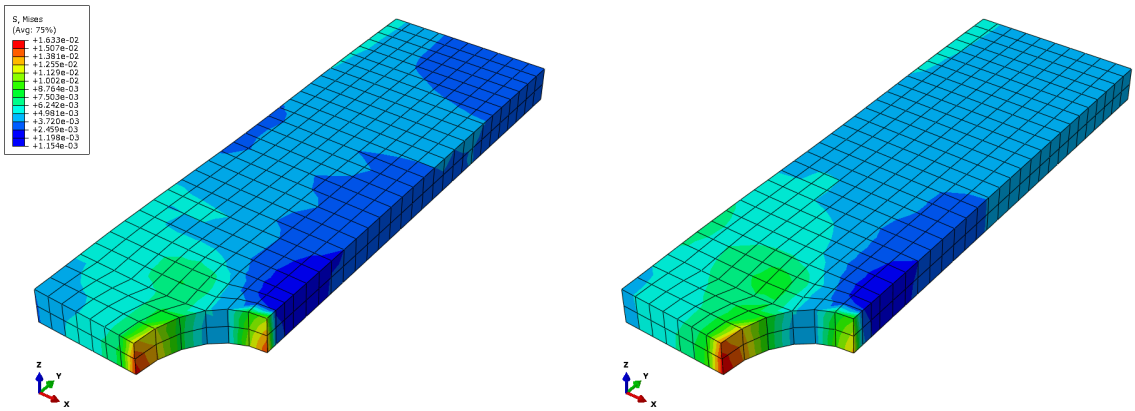


Figure 10: Comparison of isotropic and anisotropic von Mises stresses

In Figure 10 the resulting von Mises stresses under applied displacements in longitudinal direction are compared. These plots reveal that the anisotropy model yields a softer response and also a smoother stress distribution is observed. Furthermore, the strains and stresses at the upper left corner of the structure in longitudinal direction are compared in Figure 11. Due to the scaling, see equation (40), both approaches yield similar stresses in longitudinal

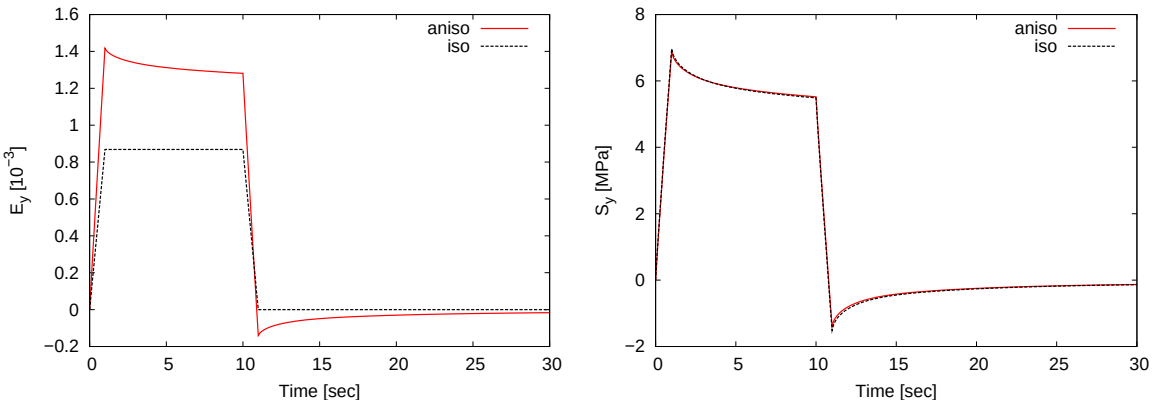


Figure 11: Comparison of strains (left-hand side) and stresses(right-hand side) in longitudinal direction

direction. Remarkably, the anisotropic model yields a relaxation in the strains for applied constant displacements. This observation is illustrated in more detail in Figure 12. In order to give an illustration which corresponds to the results of measurements in true experiments, in Figure 13 the stress-strain diagramm in longitudinal direction is given.

Finally, the resulting stresses in x-direction are compared in Figure 14. In contrast to the longitudinal stresses, here the stress responses differ, due to the fact that the scaling of the $\gamma_j$ has been carried out with respect to another direction.

Thus, the condition that the normalized relaxation behavior of each component of the composite approaches the normalized relaxation behavior of the matrix can only be guaranteed for the anisotropic approach.

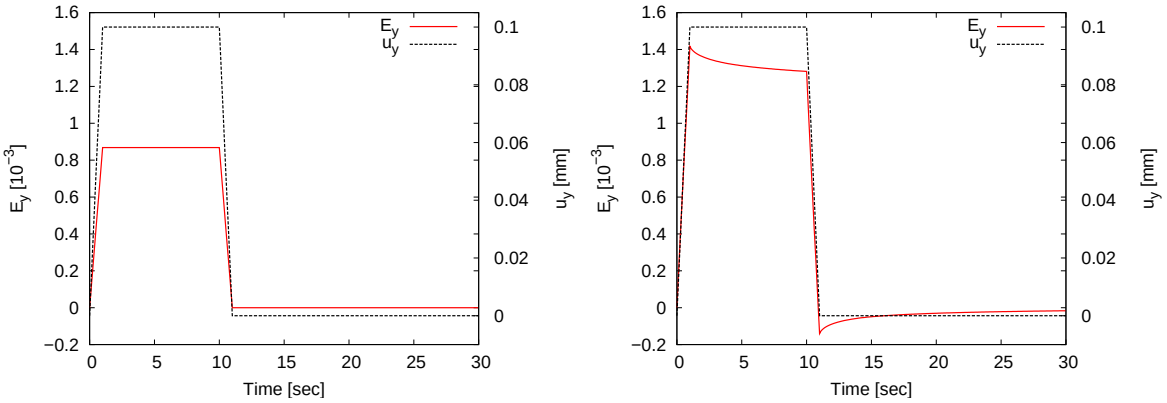


Figure 12: Comparison of displacement and strains in longitudinal direction for isotropic (left-hand side) and anisotropic (right-hand side) model

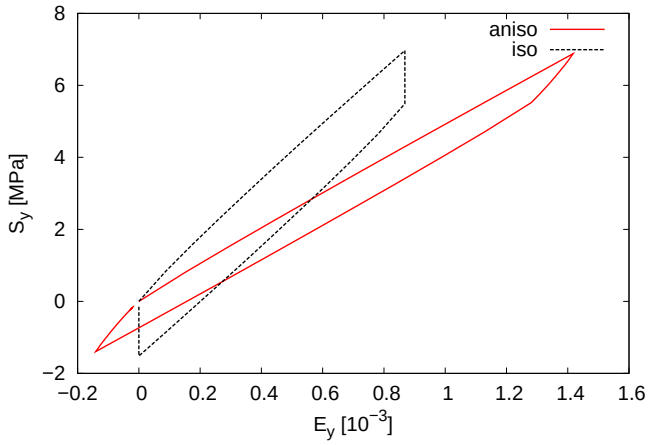


Figure 13: Stress-strain diagramm in y-direction

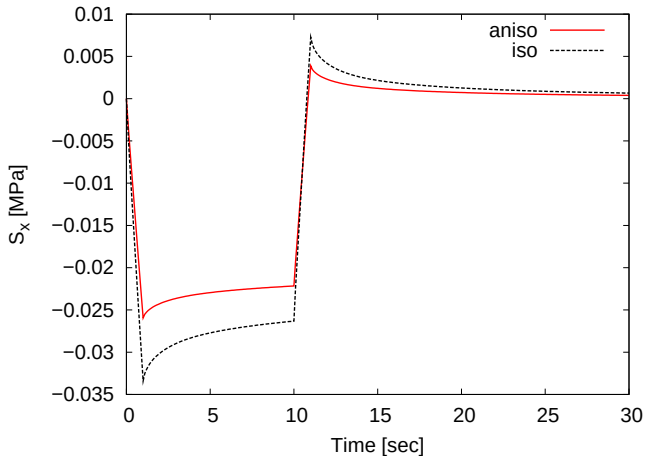


Figure 14: Comparison of stresses in x-direction

## 5 Conclusion

In the current work an approach for the simulation of the macroscopic anisotropic viscoelastic behavior of fiber-reinforced composites has been presented such that it can be implemented in standard finite element tools like ABAQUS. An advantage of the applied method is that the local influence of the fibers like orientation and volume fraction can be considered in the applied macro-scale finite element scheme. The influence of the fibers can be

captured by elastic homogenization procedures in the preprocessing. Due to this preprocessing step the method is currently limited to the linear case, nevertheless extensions to the non-linear case based on incermental schemes are an open topic for further research. Thus, the developed method yields an efficient way to simulate time-dependent macroscopic material behavior based on the local properties without a time consuming scale-transition at computation time.

**Acknowledgment**

The research was sponsored by the German Federal Ministry of Education and Research within Project No. 03X0513F (MISES-FOK) and by the Foundation for Innovation of Rhineland-Palatinate within the Project MUSSEH. Furthermore, the authors would like to thank Inga Shklyar for perfoming the ABAQUS simulations.

**References**

Advani, S. G.; Tucker, C. L.: The use of tensors to describe and predict fiber orientation in short fiber composites. *Journal of Rheology*, 31, (1987), 751–784.

Böhlke, T.; Jöchen, K.; Piat, R.; Langhoff, T.-A.; Tsukrov, I.; Reznik, B.: Elastic properties of pyrolytic carbon with axisymmetric textures. *Technische Mechanik*, 30, (2010), 343–353.

Carbon Composites: Composites-Marktbericht (2010), Carbon Composites e.V., AVK, e.V.

deBotton, G.; Tevet-Deree, L.: The response of a fiber-reinforced composite with a viscoelastic matrix phase. *Journal of Composite Materials*, 38, (2004), 1255–1277.

Feyel, F.; Chaboche, J. L.: $FE^2$ multiscale approach for modelling the elastoviscoplastic behaviour of long fibre SiC/Ti composite materials. *Computer Methods in Applied Mechanics and Engineeing*, 183, (2000), 309–330.

Hill, R.: Elastic properties of reinforced solids: Some theoretical principles. *Journal of the Mechanics and Physics of Solids*, 11, (1963), 357–372.

Holzapfel, G. A.: *Nonlinear solid mechanics*. Wiley, Chichester (2001).

Iorga, L.; Pan, Y.; Pelegri, A.: Numerical characterization of material elastic properties for random fiber composites. *Journal of Mechanics of Materials and Structures*, 3, (2008), 1279–1297.

Kaliske, M.; Rothert, H.: Formulation and implementation of three-dimensional viscoelasticity at small and finite strains. *Computational Mechanics*, 19, (1997), 228–239.

Kouznetsova, V.; Brekelmans, W. A. M.; Baaijens, F. P. T.: An approach to micro-macro modeling of heterogeneous materials. *Computational Mechanics*, 27, (2001), 37–48.

Krzikalla, F.; Zemitis, A.; Andrä, H.; Latz, A.: Simulation-based elastic upscaling of random fiber composites. *European Journal of Mechnanics A*, submitted for publication.

Lakes, R. S.; Wineman, A.: On Poisson's ratio in linearly viscoelastic solids. *Journal of Elasticity*, 85, (2006), 45–63.

Malvern, L. E.: *Introduction to the mechanics of a continuous medium*. Prentice-Hall, New Jersey (1969).

Mura, T.: *Micromechanics of Solids with Defects*. Martinus Nijhoff Publishers, Dortrecht (1987).

Nemat-Nasser, S.; Hori, M.: *Micromechanics: Overall Properties of Heterogeneous Materials*. North-Holland, Amsterdam (1999).

Ricker, S.: *Multi-scale modelling and simulation in configurational mechanics*. Ph.D. thesis, University Kaiserlautern, Germany (2011).

Wiegmann, A.; Rief, S.; Latz, A.: Geodict and filterdict: Software for the virtual material design of new filter media. Technical report, Fraunhofer ITWM (2006).

---

*Address:* Dr. Sarah Staub, PD Dr. Heiko Andrä, Dr. Matthias Kabel and Tobias Zangmeister, Fraunhofer-Institut für Techno- und Wirtschaftsmathematik (ITWM), D-67633 Kaiserslautern.
email: sarah.ricker@itwm.fraunhofer.de